ELSEVIER

Journal of Hazardous Materials B128 (2006) 130–137

Journal of Hazardous Materials

www.elsevier.com/locate/jhazmat

Oxidation of gas phase trichloroethylene and toluene using composite sol–gel TiO_2 photocatalytic coatings

Mehrdad Keshmiri [a,*], Tom Troczynski [a], Madjid Mohseni [b]

[a] *Department of Materials Engineering, University of British Columbia, 309-6350 Stores Rd., Vancouver, BC, Canada V6T 1Z4*
[b] *Department of Chemical and Biological Engineering, University of British Columbia, 2216 Main Mall, Vancouver, BC, Canada V6T 1Z4*

Received 9 March 2005; received in revised form 20 July 2005; accepted 22 July 2005
Available online 8 September 2005

Abstract

The previously developed composite sol–gel (CSG) process is proposed for the deposition of thick (10–50 μm) porous films of photocatalytic TiO_2. The CSG titania was developed by binding pre-calcined TiO_2 particles with TiO_2 sol. It had relatively high surface area (15–35 m^2/g) and good resistance against mechanical stress and abrasion. Photocatalytic activity tests were carried out on trichloroethylene (TCE) and toluene, and compared with those of standard Degussa P-25 titania. The CSG photocatalyst provided good photo-efficiency in removing both pollutants from contaminated air streams. When compared with P-25 titania, the CSG photocatalyst showed a similar photo-efficiency with first-order kinetic rate constants not significantly different from that of P-25. For both photocatalysts the rate of photocatalytic oxidation of TCE was significantly greater than that obtained for toluene. Overall, the combination of better mechanical integrity, resistance against abrasion, and comparable photocatalytic efficiency of the CSG titania versus that of P-25 titania, make the composite sol–gel (CSG) photocatalyst a viable alternative for industrial applications where long term stability, superior mechanical properties, and good photo-efficiency are of critical value.

Keywords: Photocatalysis; TiO_2; Composite sol–gel; Volatile organic compounds; Toluene; Trichloroethylene

1. Introduction

Titanium dioxide (TiO_2) heterogeneous photocatalyst has been extensively investigated in the past two decades [1–3]. The relatively high photo-efficiency of TiO_2 in decomposing organic and some inorganic pollutants, as well as its low cost, biocompatibility, and non-toxicity have made this material one of the best candidates for environmental treatments, and purification purposes [4–7]. Different forms of TiO_2, such as thin and thick film coatings, powders, and membranes have been utilized to make this catalyst more efficient and more applicable. Previous studies have indicated that the method of TiO_2 photocatalyst production and its physical form are among the most determining parameters influencing the overall photo-efficiency [8–15].

Sol–gel processing is a common chemical approach to produce high purity materials shaped as powders, coatings, fibers, monoliths, and self-supported bulk structures [8,10–12]. Through controlled hydrolysis and polycondensation reactions of a precursor (e.g. metal alkoxide) a three-dimensional network structure can be developed in the form of a gel. Subsequent drying and calcination steps may result in an oxide structure, which consolidates at sintering temperatures much lower than that of materials derived from conventional methods. For instance, the sol–gel-derived TiO_2 may be sintered at temperatures as low as 600 °C, as opposed to the "conventional" TiO_2 powders requiring 1400–1500 °C [16–20]. Through the sol–gel processing a number of determining properties of the final product such as homogeneity, purity, microstructure (in particular porosity and surface area), can be controlled better than for the conventional ceramic powders. The ability of shaping the synthesized materials in different forms (by controlling the gelation conditions, and sol viscosity) is also considered as the advantage

* Corresponding author. Tel.: +1 604 822 6304/3122; fax: +1 604 822 3619.
E-mail address: keshmiri@interchange.ubc.ca (M. Keshmiri).

0304-3894/$ – see front matter © 2005 Elsevier B.V. All rights reserved.
doi:10.1016/j.jhazmat.2005.07.060

of the sol–gel processing. However, the high shrinkage of sol–gel films or monoliths during drying and calcination frequently leads to cracking. In order to avoid this, a number of factors such as the rates of gelation, drying, and heating, the solid content of the sol, as well as component geometry (e.g. film thickness) have to be taken into account [21–26].

Photocatalyst TiO_2 has been produced in the two common forms of coatings and powders. Powders of TiO_2, particularly the sol–gel-derived powders, usually contain nano- and micro-crystallites and therefore have a relatively high surface area (up to 500 m^2/g), and consequently a high catalytic efficiency. Hence, slurries of TiO_2 have been applied widely in the field of heterogeneous photocatalysis [13,14,27,28] frequently in the forms of a suspension, and a coating. It is however observed that such coatings bond poorly to the substrate and usually do not possess sufficient mechanical integrity and therefore, are subject to rapid attrition. On the other hand, if the photocatalyst is used as a powder (i.e. suspension of the TiO_2 particles), complications such as the need for filtration and separation of the powder from the treated media (liquid or gas) are considerable. Therefore, in many applications the use of immobilized (stabilized) form of structurally bound TiO_2 on a stationary support is preferred [30,37]. We have demonstrated before that sol–gel-derived thin films of TiO_2 with thickness of ∼200 nm exhibit high bonding strength to the substrate and their resistance to abrasion (or attrition) [29]. However, the relatively low surface area of the deposited layer effectively limits the photo-efficiency of such thin coatings. As a result, these kinds of coatings of titanium dioxide have not been considered as good candidates for large-scale applications, such as purification of water or air.

In our previous study [30], a new form of TiO_2 photocatalyst coating was developed to overcome the aforementioned limitations. A previously developed processing method of producing sol–gel-derived composites of photocatalyst TiO_2 was utilized [30], wherein pre-calcined TiO_2 fine (0.02–0.1 μm) particles were used as the filler in the composite structure, bonded with the gel-derived TiO_2. The resulting coating has porous microstructure (Fig. 1), and therefore is resistant to cracking during drying and heat treatment. Also, as compared to the free-flowing powder, the developed composite exhibits good photocatalytic efficiency. The scratch removal test showed a remarkable stability, and integrity of the thick film (∼20 μm) coatings attached to the soda-lime glass substrates [29,30]. In the present work the photo-efficiency of the CSG TiO_2 photocatalyst coatings was systematically evaluated in decomposing toluene and trichloroethylene (TCE) from contaminated air streams, in a controlled differential photoreactor. Toluene and TCE were selected as model compounds because of their industrial significance and because they are common pollutants in many soil remediation and groundwater contamination sites. Also, these two compounds represent less biodegradable volatile organic compounds (VOCs) that cannot be easily treated using conventional and low cost biological treatment techniques. The efficiency of the sol–gel composites developed in this research was compared against that of Degussa P-25 TiO_2, which is a standard photocatalyst used in many investigations.

2. Experimental

2.1. Composite sol–gel photocatalyst preparation

The preparation steps for the composite sol–gel TiO_2 are described in detail elsewhere [29,30]. Titanium tetraisopropoxide ($Ti(OPr)_4$ or TTIP) (Aldrich, 97%), the precursor, was used without further purification. Anhydrous ethyl alcohol was used as the solvent to prevent fast hydrolysis of titanium alkoxide. Double-distilled deionized water was first added to the alcohol followed by HCl (Fisher, 36.5%) addition while the solution was vigorously stirred. HCl catalyst was used to control the rate of condensation and to prevent fast gelation of the sol. Hydrolysis was carried out by drop wise addition of the TTIP precursor to the prepared solution, while stirring. Pre-calcined commercial TiO_2 powder, Degussa P-25 (5 wt.%), was used as filler mixed with the sol to prepare the CSG-coating. TiO_2 powder was ultrasonically dispersed into the sol. The stability and viscosity of the suspension were controlled by altering the powder concentration and sol pH. The prepared mixture was deposited on the microscope glass slides by spin-coating technique (∼1200 rpm). The coated samples were dried at room temperature for 1 day, and then heat-treated at 500 and 700 °C for 1 h. The heating up and cooling down rates for all the samples was 6, and 2 °C/min, respectively.

2.2. Photocatalyst characterization

Microstructures of the prepared samples, after being coated with gold, were observed by SEM Hitachi S-4000N and S-4700-II, at the voltage of 20 kV, and working distance of minimum 4 mm for the highest magnification. Qualitative analyses of the resulting polymorphs of TiO_2 were carried out by the use of a Siemens-Diffraktometer D5000 at 40 kV, 40 mA (Cu Kα = 1.542 Å) at an angle of 2θ from 15 to 60°. The scan speed was 1°/min. The strongest peaks of TiO_2 corresponding to anatase (1 0 1) and rutile (1 1 0) were selected to evaluate the crystallinity of the samples. The mean crystallite size L was determined from the broadening β of the most intense line, for each polymorph, in the X-ray diffraction pattern, based on the Scherer equation:

$$L = \frac{k\lambda}{\beta \cos \theta} \quad (1)$$

where λ is the radiation wavelength, $k = 0.90$, and θ is the Bragg angle. The anatase and rutile contents in the samples were calculated from the equation:

$$f = \left(\frac{1 + 1.26 I_R}{I_A}\right)^{-1} \quad (2)$$

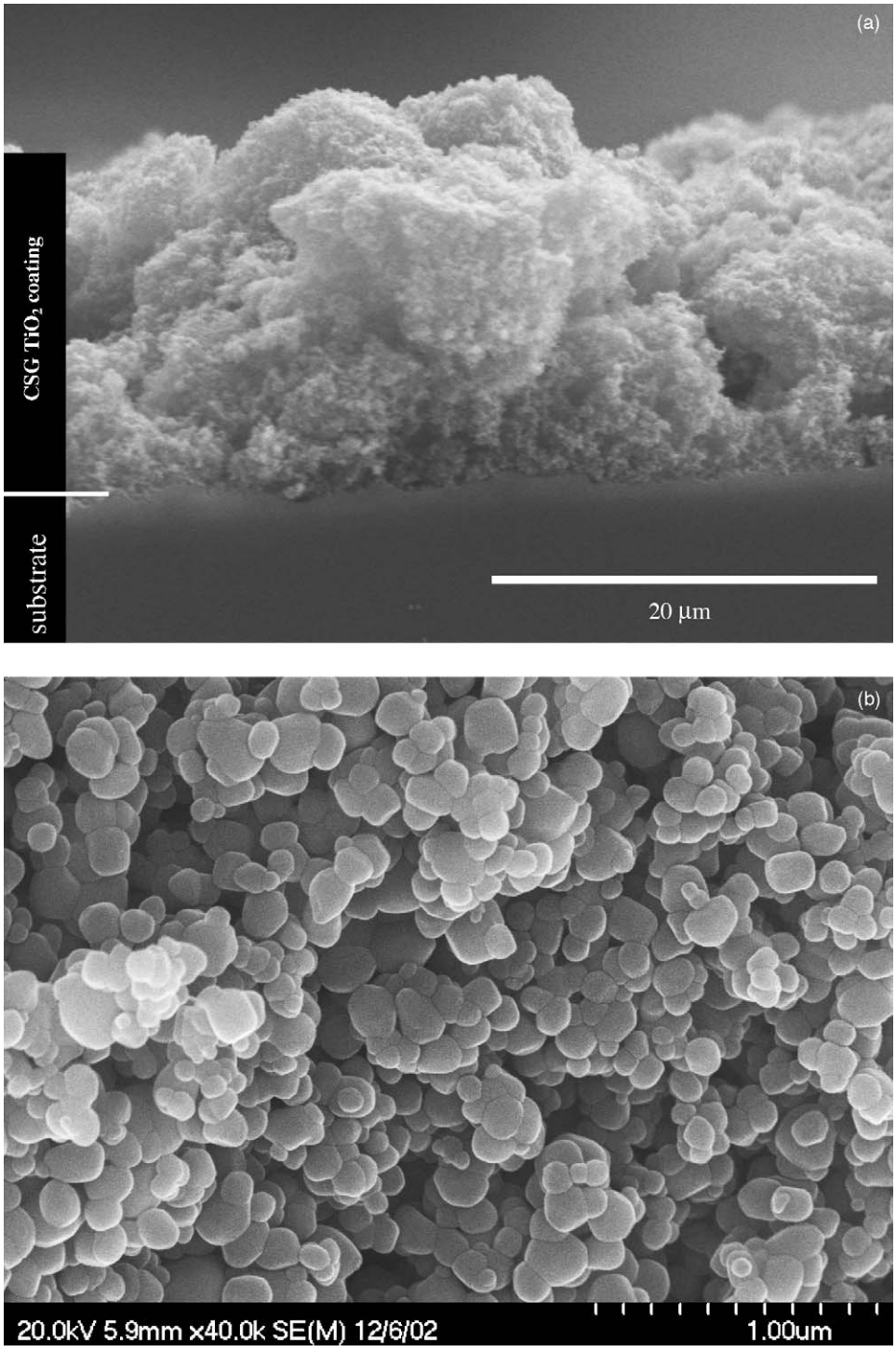

Fig. 1. (a) SEM cross-section micrograph shows the microstructure of the CSG-coating after heat treatment at 700 °C for 1 h; (b) large-magnification SEM micrograph of the CSG-coating sample shown in (a).

where f is the weight fraction of anatase in the sample, while I_A and I_R are the X-ray intensities of the anatase and rutile strongest peaks, respectively [31].

Single-point Brunauer–Emmett–Teller (BET) measurements with nitrogen as the adsorption molecule (Micromeritics FlowSorb II 2300) were used to determine the surface area of the samples. N_2 (30%) in He was used as the adsorption gas. To evaluate the surface area of the coatings, the coated layer was removed off the substrate using a sharp blade and then analyzed using the BET surface area analyzer. All measurements were made on approximately 1 g samples, which were heated at 60 °C for several days prior to testing. To

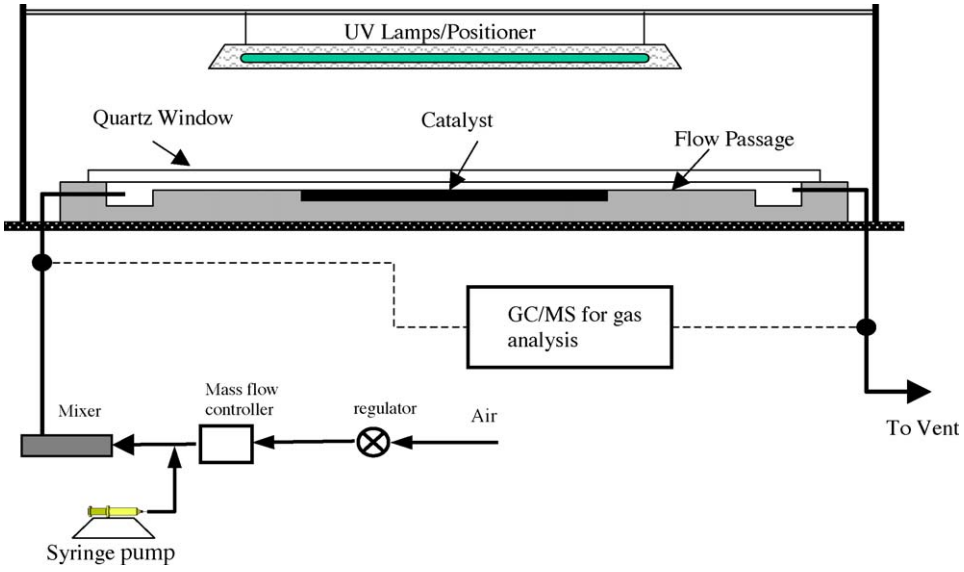

Fig. 2. Schematic diagram of the experimental set-up for photocatalytic reactions studies.

prevent any possible crystallization in the dried gel, higher drying temperatures were avoided. Test specimens were outgassed for 2 h and cooled to liquid nitrogen temperature prior to the test.

2.3. Photocatalytic activity tests

All photocatalytic activity experiments were carried out using an experimental set-up similar to that described elsewhere [30,32]. It consisted of a 25 mm wide aluminum reactor that allowed for the contaminated air to flow over the photocatalyst, Fig. 2. The photocatalyst-coated glass plates were placed in the 25 mm well, milled from the aluminium block and covered by quartz window. Gaskets between the quartz window and aluminium block created a flow passage of 25 mm (width) by 3 mm (height) above the photocatalyst glass plates. Monochromatic germicidal lamps ($\lambda = 254$ nm) or black light lamps ($\lambda = 365$ nm) provided UV illumination to the photocatalysts. The light intensity was controlled by adjusting the distance between the lamp and the catalyst surface. UV intensities were measured by a research radiometer (IL1700, International Light Inc., SED240 detector for $\lambda = 254$ nm and SED033 detector for $\lambda = 365$ nm).

Toluene and TCE were purchased as analytical reagent grade (Fisher-certified ACS). Toluene or TCE contaminated flow was generated using a syringe pump that allowed for the introduction of pure pollutant into a stream of clean air (pressurized building air) controlled by a mass flow controller, Fig. 2. The polluted stream subsequently entered the photoreactor. The retention times and inlet concentrations were adjusted using the mass flow controller for air and the injection rate of the syringe pump, respectively.

Gas samples were taken from the inlet and outlet streams and analyzed for the primary contaminant (i.e. toluene or TCE). Stainless steel tubing (1/16″ i.e. 1.6 mm diameter) was used for online samplings from the inlet and outlet streams. Gas analysis was conducted using a gas chromatograph equipped with a mass spectrometer detector (GC/MS, Saturn 2200, Varian Inc.) and a megabore capillary column (CPSil-8 CP5860). The injector temperature was 200 °C. The initial column temperature was 50 °C and it was held constant for 2 min, after which it was increased to 110 °C at a rate of 40 °C/min. Gas samples were injected into the GC/MS using a six-port sampling/injection valve (Valco Instruments Co. Inc., Huston, TX). At least three replicate samples were injected into the GC/MS.

For a differential reactor, the oxidation rate could be directly estimated from changes in the concentrations of pollutant (TCE or toluene) as shown by [30,32]:

$$r = \frac{(C_{in} - C_{out})Q}{A} \quad (3)$$

where r (g/m^2/h) is the oxidation rate, C_{in} and C_{out} (g/m^3), the inlet and outlet concentrations, respectively, Q (m^3/h), the volumetric flow rate, and A (m^2) is the surface of the photocatalyst exposed to UV irradiation.

To ensure the glass plate reactor operated in differential mode, the fractional changes of pollutant concentrations were monitored to be less than 10% for all the experiments. Also, control experiments were carried out in the absence of a photocatalyst and under direct photolytic conditions. The results showed no significant oxidation of TCE and toluene during the photolysis experiments, indicating that any removals obtained during the photocatalytic oxidation tests (using CSG and P25 photocatalysts) were due to the presence of photocatalysts and reactions involving OH (and/or other) radicals generated on the surface of the photocatalysts.

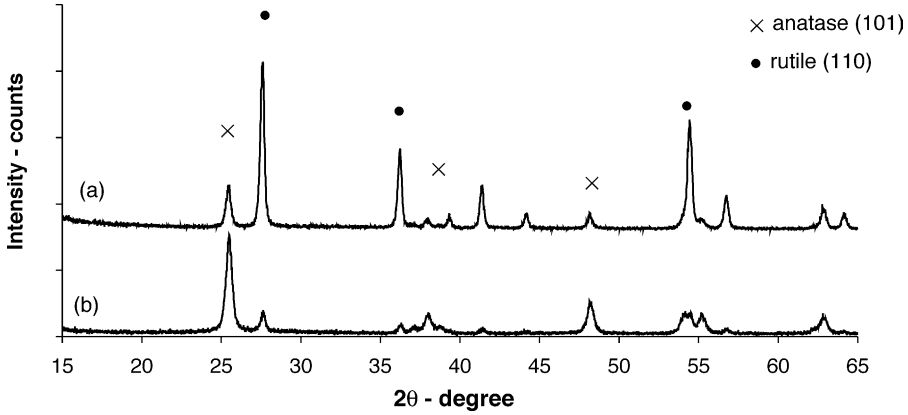

Fig. 3. XRD patterns of TiO_2 powders: (a) Degussa P-25 powder and (b) the CSG TiO_2 coating.

3. Results and discussion

3.1. 3.1 Effect of heat treatment temperature on the catalyst properties

The XRD patterns of the commercially calcined Degussa P-25 TiO_2 powder, and the CSG TiO_2 coating are shown in Fig. 3. It was shown previously [30] that the sol–gel-derived material, prior to the calcination process, had an amorphous (and/or an ultra-fine crystalline) structure, showing a very broad peak at about $2\theta = 25°$ (which is identified as the most intensive peak (1 0 1) for the anatase TiO_2). The anatase characteristic peaks became sharper, as the calcination temperature increased. The phase transformation, from anatase to rutile, took place at temperatures as low as 300 °C. The commercial powder (Degussa P-25, in as-received state with approximately 80% anatase and 20% rutile) phase transformation, from anatase to rutile, apparently initiated at 500–600 °C [33]. In this study, 700 °C was the maximum temperature used for CSG preparation as it was sufficient for ceramic bond formation to assure the desired structural integrity and adhesion of the CSG titania photocatalyst.

The specific surface area of P-25 was reduced by about 50% when heated to 700 °C for 1 h (Table 1). This indicates partial sintering of the powder, leading to shrinking of the agglomerates and reduction in the size of the fine pores. This, as a result, affected the surface area of the CSG-coating, which decreased to ~60% of its initial value, after heating at 700 °C for 1 h.

The normal loads which caused the complete coating removal, for P-25 and CSG samples, within the scratch track (observed by optical microscope) are shown in Table 1. For P-25 TiO_2 powder coating deposited from a slurry (i.e. without the sol binder), the normal load needed to remove the coatings from the substrate was in the range of 0–0.2 N. These powder slurry deposited coatings show also no change (i.e. no increase) in their adhesion strength after firing up to 700 °C for 1 h. However, as shown in Table 1, the load required for the complete removal of the TiO_2 CSG-coating, increases considerably due to the calcination treatment.

Table 1
Physical and chemical characteristics of CSG TiO_2 coating, compared to P-25 photocatalyst

Material	Heat treatment conditions	Anatase (%)	Surface area (m^2/g)	L^a (N)
Degussa P-25	–	78	45.21	~0
	500 °C, 1 h	70	40.04	~0
	700 °C, 1 h	43	28.31	0.170
CSG-coating	–	75	22.11	0.230
	500 °C, 1 h	75	34.33	6.14
	700 °C, 1 h	17	14.61	10.6

[a] Critical linearly increasing loads.

3.2. Effect of gas flow rate

Gas flow rate is one of the important process parameters affecting the rate of photocatalytic oxidation. It affects gas phase mass transfer and the transport of pollutants to the catalyst surface where oxidation takes place. The effect of flow rate on the oxidation rate of TCE in the glass plate differential photoreactor is shown in Fig. 4. The rate of TCE oxidation

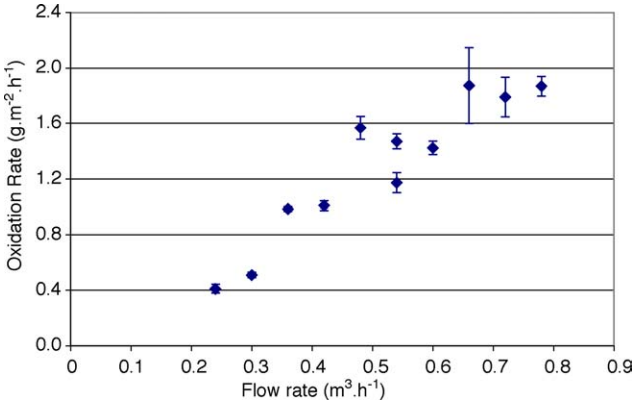

Fig. 4. Effect of gas flow rate on the TCE oxidation rate within the differential photoreactor.

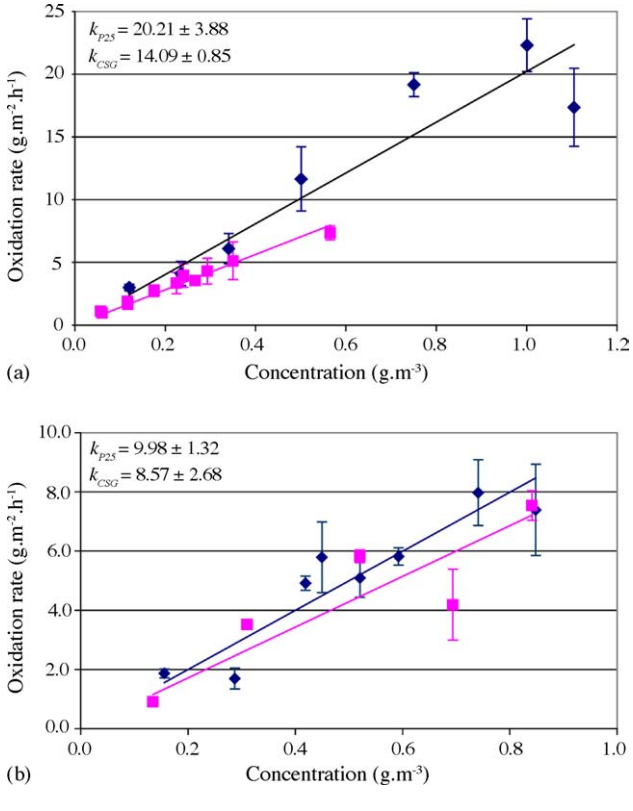

Fig. 5. Photocatalytic oxidation rate for TCE (♦) P-25, (■) CSG-coating: (a) 254 nm low pressure UV source; (b) 365 nm low pressure UV source. k_{P25} and k_{CSG} represent the first-order rate constants for the P-25 and CSG-coating photocatalysts, respectively.

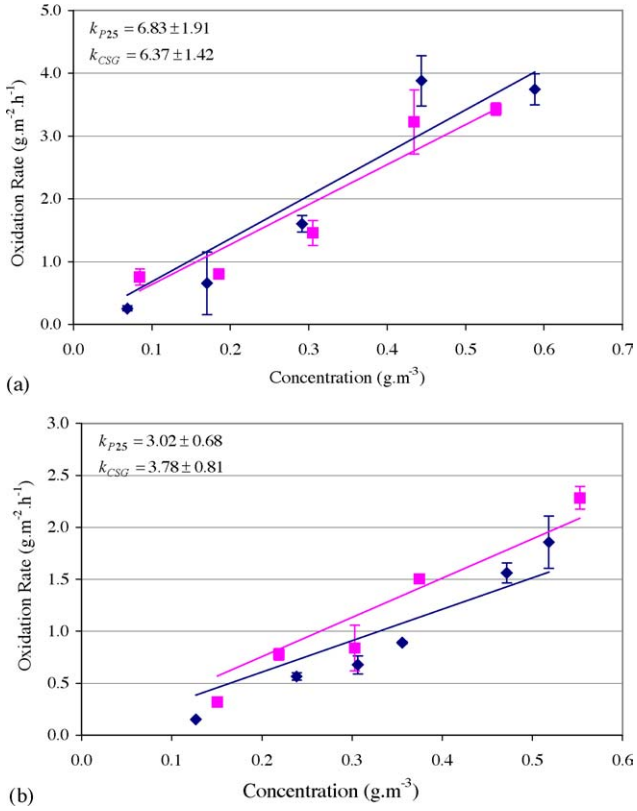

Fig. 6. Photocatalytic oxidation rate for toluene (♦) P-25, (■) CSG-coating: (a) 254 nm low pressure UV source; (b) 365 nm low pressure UV source. k_{P25} and k_{CSG} represent the first-order rate constants for the P-25 and CSG-coating photocatalysts, respectively.

increased with flow rate up to about 0.65 m^3/h. The direct effect of flow rate on PCO rate indicates that mass transfer plays an important role and that the rate of oxidation is limited by mass transfer. Higher flow rate enhances turbulence in the reactor and increases gas phase mass transfer, bringing more pollutants to the photocatalyst surface. As the flow rate increased and mass transfer limitation decreased, the rate of oxidation levelled off and stayed constant, Fig. 4. In other words, beyond 0.65 m^3/h there was no mass transfer limitation. This information was invaluable for further experiments as it allowed us to conduct proper experiments on determining the intrinsic kinetics for the degradation of pollutants (i.e. TCE and toluene) in the glass plate differential photoreactors.

3.3. Rates of TCE and toluene photocatalysis

Figs. 5 and 6 show the intrinsic PCO rates of TCE and toluene, respectively, obtained at 0.72 m^3/h gas flow rate. For toluene, the CSG-coating provided photocatalytic activities comparable to that of the standard photocatalyst P-25 titania. In other words, comparison between oxidation rates of toluene using two different photocatalysts and two UV sources (shown in Fig. 6) suggests that there was little difference between the performance of these two photocatalysts and both systems provided similar contaminant removal efficiencies. For TCE photocatalysis, however, P-25 titania and CSG photocatalyst performed differently when 254 nm UV source was used (Fig. 5a). Although P-25 and CSG photocatalysts performed similarly under 365 nm UV irradiation, P-25 photocatalyst provided higher TCE degradation than the CSG-coating. The kinetic rate constant obtained for P-25 titania was 50% larger than that for CSG-coating. It is not quite understood why P-25 performed slightly better under this particular condition, while both photocatalyst performed similarly under other experimental conditions. One possible speculation could be the contribution of free radicals (i.e. chlorine free radicals) that are generated during the photocatalysis of TCE with germicidal (i.e. 254 nm) UV irradiation. Higher surface area associated with P-25 titania (see Table 1) might contribute to significantly greater Cl radical subtraction, resulting in higher rates of TCE oxidation.

Another similar observation is related to the oxidation rate obtained by both P-25 and CSG photocatalysts that followed first-order kinetics over the range of inlet concentrations (up to about 1.0 g/m^3) tested in the photoreactor. This is in agreement with previous studies [30,34], indicating that PCO rates follow first-order kinetics at low concentrations and approach zero-order with increasing the concentration of pollutants in the air. In addition, the order of PCO was not dependent upon

the source of UV irradiation and both 254 and 365 nm UV resulted in first-order kinetics.

The first-order rate constants obtained for each contaminant and UV irradiation wavelength can be compared using the information in Figs. 5 and 6. The rate of PCO for TCE was significantly greater than that for toluene (Fig. 5). A combination of OH and Cl radical-initiated/sensitized oxidations was likely responsible for these greater rate constants [35]. For the PCO of toluene, the rate was smaller because both direct hole transfer to the compound and H abstraction by OH radicals are relatively small [36], especially compared to the Cl radical-initiated oxidation during the PCO of TCE. Chlorine radicals have already been proven to accelerate the chain reaction during the PCO of TCE, resulting in significantly higher removal rates [35]. Figs. 5b and 6b also show that PCO rate constants offered by 365 nm UV were lower than those resulted from 254 nm UV. Although both 254 and 365 nm UV sources possess enough ionization energy to overcome the band gap energy of anatase titania (3.2 eV) and generate charged carriers (electron-hole pairs) required for initiating the oxidation reactions, the higher lamp intensity was likely the primary reason for the higher PCO rates obtained using 254 nm UV source (3.05×10^{-3} W cm^{-2} for UV 254 nm versus 2.13×10^{-3} W cm^{-2} for UV 365 nm).

Overall, the performance of the CSG-coatings prepared by sol–gel technique is comparable to that offered by P-25 which is a well-established photocatalyst. At the same time, better mechanical integrity and abrasion resistance offered by the CSG-coating photocatalyst (Table 1) makes it a viable alternative to P-25 for large-scale commercial applications that require long term operations under sometimes abrasive environmental conditions.

4. Conclusions

This research focused on developing and evaluating the composite sol–gel (CSG) TiO_2 photocatalyst obtained from binding pre-calcined photocatalytic TiO_2 particles with TiO_2 sol. The CSG photocatalyst provided relatively high surface area (15–35 m^2/g) and good resistance against mechanical stress and abrasion. It also provided good photo-efficiency at removing two common air pollutants (TCE and toluene). The photocatalytic activity of the CSG was comparable to that of standard Degussa P-25 titania. The rate of photocatalytic oxidation of TCE was significantly greater than that obtained for toluene. In addition, when tested with two UV sources of 254 and 365 nm, 254 nm UV source provided higher PCO for both contaminants. The better mechanical integrity and resistance against abrasion, along with comparable photocatalytic efficiency to that of P-25 titania, makes the composite sol–gel photocatalyst developed in this research a viable alternative for industrial and large-scale applications where long term stability, superior mechanical properties, and good photo-efficiency are of critical value.

Acknowledgements

The authors would like to acknowledge the Natural Sciences and Engineering Research Council (NSERC) of Canada for financial support. GC/MS was purchased through funding from Canada Foundation for Innovation (CFI) new opportunity fund and British Columbia Knowledge Development Fund (BC KDF). Mehrdad Keshmiri was supported by the Science Council of British Columbia “Great Award” scholarship program.

References

[1] A. Fujishima, T.N. Rao, D.A. Tryk, Titanium dioxide photocatalysis, J. Photochem. Photobiol. C: Photochem. Rev. 1 (2000) 1.
[2] M.R. Hoffmann, S.T. Martin, W. Choi, D.W. Bahnemann, Environmental applications of semiconductor photocatalysis, Chem. Rev. (1995) 6.
[3] J.C. Crittenden, Y. Zhang, D.W. Hand, D.L. Perram, E.G. Marchand, Solar detoxification of fuel-contaminated groundwater using fixed-bed photocatalysts, Wat. Environ. Res. 68 (1996) 270.
[4] J. Grzechulska, M. Hamerski, A.W. Morawski, Photocatalytic decomposition of oil in water, Wat. Res. 34 (2000) 1638.
[5] J. Arana, J.A.H. Melian, J.M.D. Rodrigez, O.G. Diaz, A. Viera, J.P. Pena, P.M.M. Sosa, V.E. Jimenez, TiO_2-photocatalysis as a tertiary treatment of naturally treated wastewater, Catal. Today 76 (2002) 279.
[6] H. Gerischer, A. Heller, Photocatalytic oxidation of organic molecules at TiO_2 particlesby sunlight in aerated water, J. Electrochem. Soc. 139 (1992) 11.
[7] J.A. Byrne, A. Davidson, P.S.M. Dunlop, B.R. Eggins, Water treatment using nano-crystalline TiO_2 electrodes, J. Photochem. Photobiol. A: Chem. 148 (2002) 365.
[8] S.-I. Nishimoto, B. Ohtani, H. Kajiwara, T. Kagiya, Correlation of the crystal structure of titanium dioxide prepared from titanium tetra-2-propoxide with the photocatalytic activity for redox reactions in aqueous propan-2-ol and silver salt solutions, J. Chem. Soc., Faraday Trans. 1 81 (1985) 61.
[9] M. Lindner, J. Theurich, D.W. Bahnemann, Photocatalytic degradation of organic compounds: accelerating the process efficiency, Wat. Sci. Technol. 35 (1997) 79.
[10] D.S. Muggli, J.T. McCue, J.L. Falconer, Mechanism of photocatalytic oxidation of ethanol on TiO_2, J. Catal. 173 (1998) 470.
[11] Y. Ohko, D.A. Tryk, K. Hashimoto, A. Fujishima, Autooxidation of acetaldehyde initiated by TiO_2 photocatalysis under weak UV illumination, J. Phys. Chem. B 102 (1998) 2699.
[12] S.A. Walker, P.A. Christensen, K.E. Shaw, G.M. Walker, Photoelectrochemical oxidation of aqueous phenol using titanium dioxide aerogel, J. Electroanal. Chem. 393 (1995) 137.
[13] S.N. Frank, A.J. Bard, Heterogeneous photocatalytic oxidation of cyanide and sulfite in aqueous solutions at semiconductor powders, J. Phys. Chem. 81 (1977).
[14] B. Kraeutler, A.J. Bard, Heterogeneous photocatalytic decomposition of saturated carboxylic acids on TiO_2 powder. Decarboxylative route to alkanes, J. Am. Chem. Soc. 100 (1978) 5985.
[15] C.A. Martin, M.A. Baltanas, A.E. Cassano, Photocatalytic decomposition of chloroform in a fully irradiated heterogeneous reactor using titanium dioxide particulate suspensions, Catal. Today 27 (1996) 221.
[16] J.L. Woolfrey, J.R. Bartlett, in: L.C. Klein, E.J.A. Pope, S. Sakka, J.L. Woolfrey (Eds.), Sol–gel processing of advanced materials, The American Ceramic Society, 1998, p. 3.
[17] J.D. Mackenzie, in: L.L. Hench, D.R. Urlich (Eds.), Science of Ceramic Chemical Processing, John Wiley & Sons, 1986, p. 113.

[18] D. Segal, Chemical synthesis of ceramic materials, J. Mater. Chem. 7 (1997) 1297.
[19] O. Bouquin, N. Blanchard, P. Colombian, in: P. Vincenzini (Ed.), High Tech Ceramics, Elsevier Science Publishers, Amsterdam, 1987, p. 717.
[20] J. livage, F. Beteille, C. Roux, M. Chatry, P. Davidson, Sol–gel synthesis of oxide materials, Acta Mater. 46 (1998) 743.
[21] C.J. Brinker, G.W. Scherer, Sol–Gel Science — the Physics and Chemistry of Sol–Gel Processing, Academic Press Inc., 1990, p. 453.
[22] G.W. Scherer, Theory of drying, J. Am. Ceram. Soc. 73 (1990) 3.
[23] G.W. Scherer, Correction of drying gells. Part I. Theory, J. Non-Cryst. Solids 92 (1987) 375.
[24] T.A. Ring, Fundamentals of Ceramic Powder Processing and Synthesis, Academic Press Inc., 1996, p. 349.
[25] C.J. Brinker, G.W. Scherer, Sol–Gel Science — The Physics and Chemistry of Sol–Gel Processing, Academic Press Inc., 1990, p. 675.
[26] R.M. German, Sintering Theory and Practice, John Wiley & Sons, NY, 1996, p. 67.
[27] N. Serpone, Relative photonic efficiencies and quantum yields in heterogeneous photocatalysis, J. Photochem. Photobiol. A: Chem. 104 (1997) 1.
[28] G.P. Fotou, S. Vemury, S.E. Pratsinis, Synthesis and evaluation of titania powders for photodestruction of phenol, Chem. Eng. Sci. 49 (1994) 4939.
[29] M. Keshmiri, Composite sol–gel process for photocatalytic TiO_2, Ph.D. Thesis, 2004, UBC.
[30] M. Keshmiri, M. Mohseni, T. Troczynski, Development of novel TiO_2 sol–gel-derived composite and its photocatalytic activities for trichloroethylene oxidation, Appl. Catal. B: Environ. 53 (2004) 209–219.
[31] R.A. Spurr, H. Myers, Quantitative analysis of anatase–rutile mixtures with an X-ray diffractometer, Anal. Chem. 29 (1957) 760.
[32] M. Mohseni, F. Taghipour, Experimental, CFD analysis of photocatalytic gas phase vinyl chloride (VC) oxidation, Chem. Eng. Sci. 59 (2004) 1601–1609.
[33] D.C. Hague, M.J. Mayo, The effect of crystallization and a phase transformation on the grain growth of nanocrystalline titania, Nanostruct. Mater. 3 (1993) 61.
[34] S. Upadhya, D.F. Ollis, A simple kinetic model for the simultaneous concentration and intensity dependencies of TCE photocatalyzed destruction, J. Adv. Oxid. Technol. 3 (1998) 199–202.
[35] M.R. Nimlos, W.A. Jacoby, D.M. Blake, T.A. Milne, Direct mass spectrometric studies of the destruction of hazardous wastes. Part 2. Gas-phase photocatalytic oxidation of trichloroethylene over titanium oxide: products and mechanisms, Environ. Sci. Technol. 27 (1993) 732–740.
[36] O. d'Hennezel, P. Pichat, D.F. Ollis, Benzene and toluene gas-phase photocatalytic degradation over H_2O and HCl pretreated TiO_2: byproducts and mechanisms, J. Photochem. Photobio. A: Chem. 118 (1998) 197–204.
[37] G. Balasubramanian, D.D. Dionysiou, M.T. Suidan, I. Baudin, J.M. Laine, Evaluating the activities of immobilized TiO_2 powder films for the photocatalytic degradation of organic contaminants in water, Appl. Catal. B: Environ. 47 (2004) 73.